



Kent Academic Repository

Everson, Mike, Duma, Virgil F. and Dobre, George (2018) *Aspects of vignetting in a polygon mirror-based spectral filter for swept source optical coherence tomography (SS-OCT)*. In: Todea, Carmen and Podoleanu, Adrian G.H. and Duma, Virgil-Florin, eds. *Seventh International Conference on Lasers in Medicine*. Proceedings of SPIE, 19 (59). SPIE. ISBN 978-1-5106-2287-6.

Downloaded from

<https://kar.kent.ac.uk/69493/> The University of Kent's Academic Repository KAR

The version of record is available from

<https://doi.org/10.1117/12.2282284>

This document version

Publisher pdf

DOI for this version

Licence for this version

UNSPECIFIED

Additional information

Versions of research works

Versions of Record

If this version is the version of record, it is the same as the published version available on the publisher's web site. Cite as the published version.

Author Accepted Manuscripts

If this document is identified as the Author Accepted Manuscript it is the version after peer review but before type setting, copy editing or publisher branding. Cite as Surname, Initial. (Year) 'Title of article'. To be published in *Title of Journal*, Volume and issue numbers [peer-reviewed accepted version]. Available at: DOI or URL (Accessed: date).

Enquiries

If you have questions about this document contact ResearchSupport@kent.ac.uk. Please include the URL of the record in KAR. If you believe that your, or a third party's rights have been compromised through this document please see our [Take Down policy](https://www.kent.ac.uk/guides/kar-the-kent-academic-repository#policies) (available from <https://www.kent.ac.uk/guides/kar-the-kent-academic-repository#policies>).

PROCEEDINGS OF SPIE

[SPIDigitalLibrary.org/conference-proceedings-of-spie](https://spiedigitallibrary.org/conference-proceedings-of-spie)

Aspects of vignetting in a polygon mirror-based spectral filter for swept source optical coherence tomography (SS-OCT)

Michael Everson, Virgil-Florin Duma, George Dobre

Michael Everson, Virgil-Florin Duma, George Dobre, "Aspects of vignetting in a polygon mirror-based spectral filter for swept source optical coherence tomography (SS-OCT)," Proc. SPIE 10831, Seventh International Conference on Lasers in Medicine, 108310L (10 August 2018); doi: 10.1117/12.2282284

SPIE.

Event: Seventh International Conference on Lasers in Medicine, 2017, Timisoara, Romania

Aspects of vignetting in a polygon mirror-based spectral filter for Swept Source Optical Coherence Tomography (SS-OCT)

Michael Everson^{1,*}, Virgil-Florin Duma^{2,3}, George Dobre¹

¹Applied Optics Group, School of Physical Sciences, University of Kent, Canterbury, CT2 7NH, United Kingdom

²3OM Optomechatronics Group, "Aurel Vlaicu" University of Arad, 77 Revolutiei Ave, Arad 310130, Romania

³Doctoral School, Polytechnic University of Timisoara, 1 Mihai Viteazu Ave, Timisoara 300222, Romania

ABSTRACT

Optical Coherence Tomography (OCT) is a technology capable of producing 3-D volumes of microscopic structures with micron-scale resolution. Its main area of application remains ophthalmology and in particular retinal imaging. The quality and usability of the images depends upon the frame rate and the properties of the light being used. Swept source OCT (SS-OCT) can offer a speed advantage; variants using polygon mirrors (PMs) as spectral filters in SS-OCT have resulted in a variety of different arrangements. Although their application has been successfully demonstrated, a more detailed study of the particular aspects and requirements of beam propagation through the filter and their overall impact on the system performance have not been reported. Examining aspects related to vignetting at the PM facet leads to maximizing light throughput and system performance, which is the aim of this work. A swept source spectral filter consisting of a transmission grating, a two-lens telescope, an off-axis PM, and an end reflector mirror has been evaluated in terms of the beam width at the PM facet and how this parameter varies across the entire width of the spectrum at the input of the spectral filter.

Keywords list: optical coherence tomography (OCT), spectral filter, polygon mirror (PM), spectral tuning, wavelength sampling.

1. INTRODUCTION

Optical Coherence Tomography (OCT) relies on low coherence interferometry to obtain structural depth information from objects that permit light propagation (even if multiply scattered) over a few millimetres in depth. It is non-invasive and is widely used, for example in ophthalmology and dentistry for clinical investigations and diagnostic purposes. Several wavelength windows, from the visible to 1500 nm can be used depending on the properties of the target, and especially on the water absorption. Particularly important is to carry out imaging *in-vivo* at speeds that avoid motion artefacts.

Swept Source OCT (SS-OCT) exhibits higher sensitivity and generally faster scanning speeds and for this reason is often preferred to alternatives such as time-domain or spectrometer-based OCT¹. In SS-OCT, a light source which emits over a wide wavelength range is passed through a spectral filter to produce narrow laser linewidths; this is done by sweeping/tuning the wavelengths over time.

One way of achieving this tuning in a repeatable manner is by utilising a spinning polygon mirror (PM)², which although bulky can perform this task at facet repetition rates of tens of kHz. As each PM facet sweeps through the region where it intercepts the angularly dispersed incoming beam, it reflects chromatic components from the original broadband spectrum – as the facet is progressively positioned at different angles. Light in a narrow subset of wavelengths is returned into the emitting fibre only if the angle condition is satisfied for that narrow range of wavelengths.

*mje23@kent.ac.uk; phone 01227 82 3288; aogkent.uk

PM-based swept sources are high versatility alternatives to MEMS-based devices. Although state-of-the-art swept source lasers are capable of producing MHz scanning frequencies³, they are typically limited in their choice of operating wavelength. A PM can operate at any wavelength within the spectral domain specific for a certain coating (e.g., gold – for a maximum reflectivity in IR) and can achieve wavelength sweeping repetition rates of >400 kHz⁴. Importantly, it is possible to operate the PM in different wavelength ranges (and multiple sources at different wavelengths whose operation is synchronised has even been realised in this way⁵). Since the same PM is used, this wavelength flexibility can be achieved at a reduced cost. As a drawback, the overall physical size of the spectral filter, substantially determined by the length of the telescope, currently constitutes a barrier to the deployment of such sources outside the laboratory.

An important parameter of a PM operation is the proportion of incident light that is successfully returned for each wavelength, for which a key factor is the phenomenon of beam vignetting at the PM facet^{6,7}. In this work, we examine how the width of the beam incident on a PM facet varies across the input broadband spectrum of light, for different eccentricities of the polygon with respect to the optical axis of the telescope.

2. ANALYSIS OF THE PM-BASED SS

2.1. Principle scheme of the PM-based SS

The total swept bandwidth and the instantaneous linewidth generated at the output of the swept source are key factors in determining the axial resolution of a SS-OCT system. The configuration we use employs a filter consisting of a transmission grating, a two-lens telescope, a PM, and an end reflector (Fig. 1).

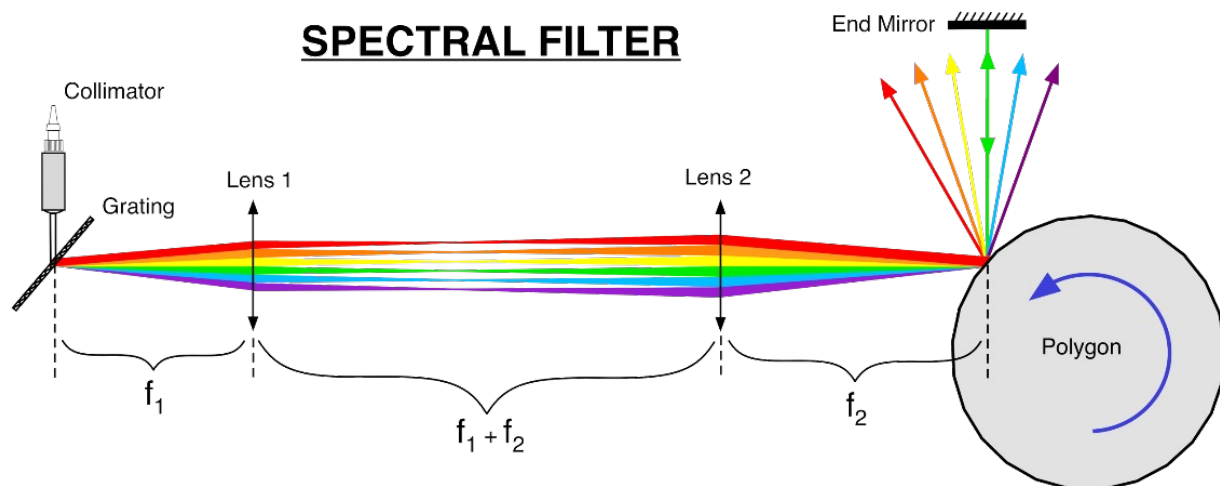


Figure 1. Experimental setup consisting of a collimator, a transmission grating, a two-lens telescope, a PM, and an end mirror. The PM rotates counterclockwise, sweeping through the spectrum from λ_{max} to λ_{min} . During a single facet rotation, each wavelength is tuned sequentially by retro-reflecting at normal incidence on the end mirror, propagating back through the filter along exactly the same path they came.

Light incident on the grating is collimated by a fibre collimator and is subsequently diffracted at various wavelength dependent angles. If the total spectrum is divided into vanishingly small wavelength intervals, one way to conceptualise the propagation through the telescope is to consider individual beams of light in each such interval. Such beams originate at the grating, come to a focus at a distance f_1 equal to the focal length of Lens 1, diverge and arrive at the PM facet collimated again. The role of the two-lens telescope is to allow light dispersed angularly by the grating to converge at the PM facet by ensuring that the grating and the active facet are optical conjugates.

Firstly, it is useful to consider briefly the case when the PM is placed on-axis, illustrated in Figure 2. In order for light of any wavelength to return along the same path and be recaptured in the original fibre, the angle of incidence on the facet needs to be 0° . This places a limit on the maximum angle of convergence ψ that can be accommodated on the facet as it rotates, given that the angle between two adjacent facets is equal to $2\pi/n$, where n is the number of facets of the PM. Therefore, the converging angle ψ in an on-axis system is limited to $2\pi/n$.

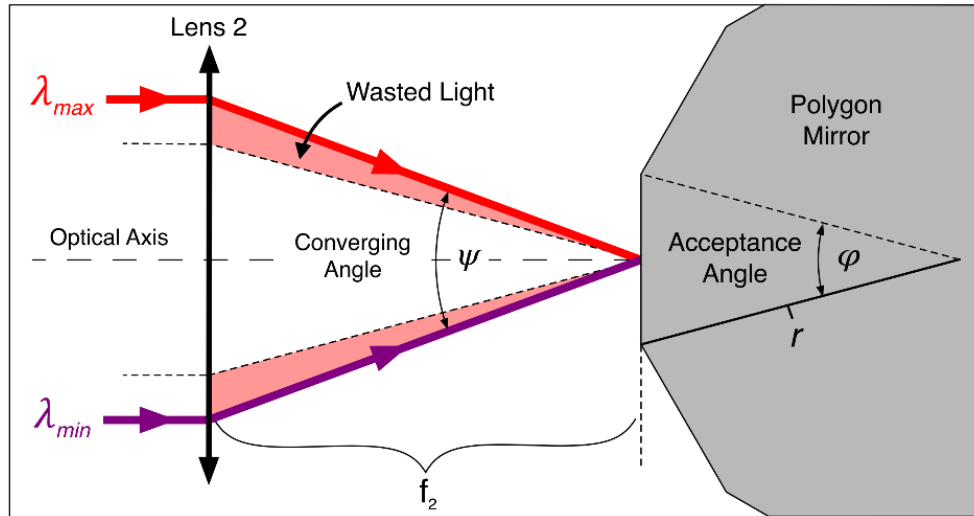


Figure 2. Example using an on-axis setup without an end mirror to highlight the necessity to match the converging angle of the spectrum to the acceptance angle of the PM. Any incident beams falling outside of this angle will not be successfully retro-reflected off the PM. Note that the light must travel exactly along the same path it came to be successfully captured by the collimator and injected back into the fibre.

By introducing an eccentricity and placing the PM off-axis, the converging angle is doubled to $4\pi/n$, which is desirable since it allows for finer tuning of individual wavelengths and hence for an improvement in the linewidth^{8,9}. The off-axis placement requires an end reflector to bounce light back along the same path. As the PM rotates, its facet fulfils the incidence angle condition sequentially from λ_{max} to λ_{min} . At any specific moment during the sweep, only light of a wavelength λ that reflects off the facet at the precise angle to send it to the end reflector with normal incidence will be travelling back along the same path and will be reinjected back into the fibre. Other wavelengths will not strike the end reflector at normal incidence and therefore will not be directed back towards the receiving fibre at the required angle.

2.2. Beam widths

The beams propagating out of the collimator change width as they emerge through the grating (Wasatch, 1310 nm, 48° operating angle) in the object space of Lens 1. This is a purely geometric property of the setup created by the different diffraction angles experienced for each wavelength. The beam width at each wavelength is found by the examination of the wavelength dependent diffraction angle $\delta_n(\lambda_n)$ given by the grating equation:

$$\delta_n = \sin^{-1}(Gm\lambda_n - \sin \gamma), \quad (1)$$

where $G = 1145 \text{ l/mm}$, $m = \text{order (1)}$, $\lambda_n = \text{wavelength}$, and $\gamma = \text{the angle of incidence on the grating } (48^\circ)$. The width of the beam in the object space of Lens 1 is denoted W_1 and has the following relationship with the initial beam width W_0 :

$$W_1 = W_0 \frac{\cos \delta_n}{\cos \gamma}. \quad (2)$$

Examining the diffraction angles over the range of wavelengths λ_{min} to λ_{max} , we find that the longest wavelength in the spectrum has the narrowest beam width and the shortest wavelength has the widest beam width (Fig. 3).

The beams are captured by the two-lens telescope, which directs them onto the target facet of the PM (Fig. 4). Previous studies have shown that these filters experience vignetting on the facets, which results in a loss of power⁶. Therefore, it is important to match the width W_2 of the beam incident on the PM to the size of a facet to avoid introducing additional vignetting. This is achieved by changing the focal lengths on Lens 1 & 2, where W_2 is given by

$$W_2 = W_1 \frac{f_2}{f_1} \tag{3}$$

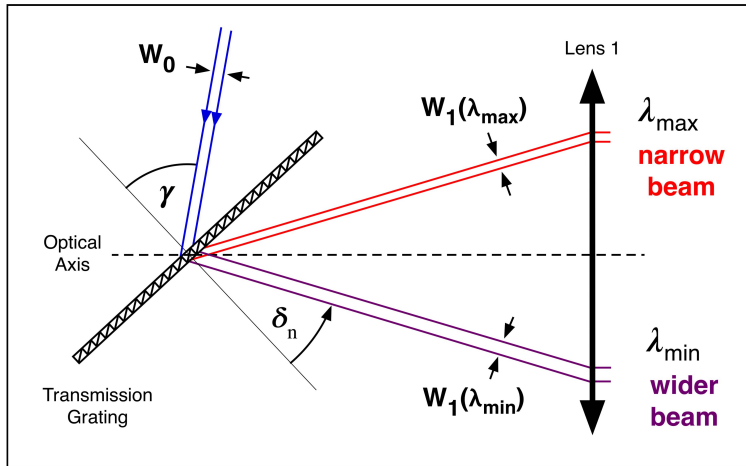


Figure 3. The spectrum is dispersed by the transmission grating into the object space of Lens 1. The orientation of the grating and the initial beams' grazing angle γ produces wider beam widths for the shortest wavelength and narrower beam widths for the longest wavelength. The widths of each beam can be found by using the grating equation to calculate the diffraction angles of each wavelength.

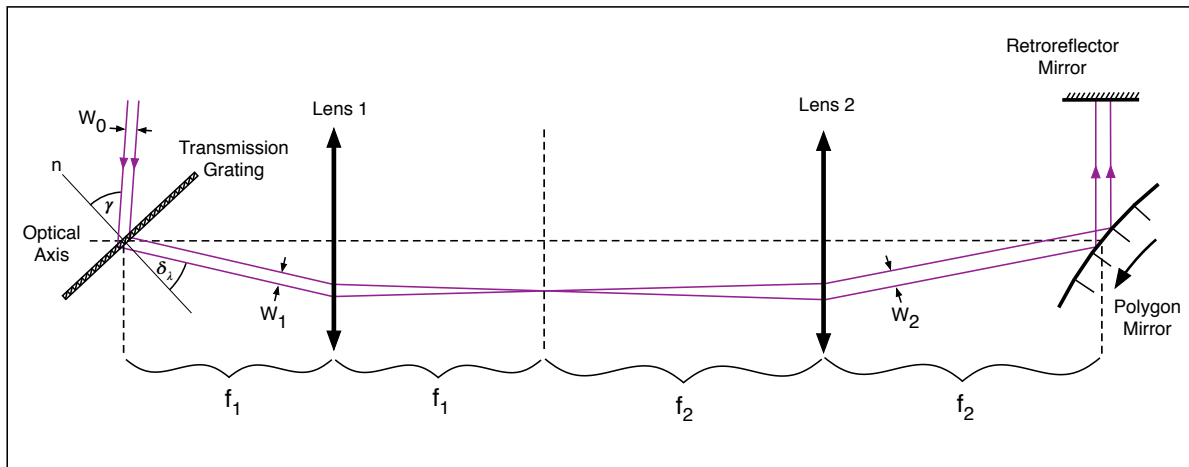


Figure 4. An example of the spectral filter tuning the shortest wavelength. The initial beam width W_0 increases to W_1 after traversing through the grating. Using a two-lens telescope with different focal lengths changes the beam width again to W_2 , which is then directed onto the PM, where it is retro-reflected off the end mirror at normal incidence.

2.3. Facet width and eccentricity

The apothem of the PM and the number of facets determine the width of each facet. The Lincoln Laser SA34 polygon mirror used in our setup has an apothem $R = 31.75$ mm and number of facets $n = 72$. The width of each facet is therefore given by

$$a = 2R \sin\left(\frac{\pi}{n}\right) \tag{4}$$

In our setup $a = 2.77$ mm. As mentioned before, in order to improve the instantaneous linewidth of the filter, the PM is positioned off-axis by introducing an eccentricity E , which is measured vertically from the optical axis to the center of the polygon. Figure 5 shows the positioning of the polygon in the ‘below-axis’ configuration. The target facet is no longer perpendicular to the optical axis but has been rotated clockwise away from normal incidence. This arrangement requires the addition of an extra mirror to act as a retroreflector. The PM must also be shifted axially towards the telescope by an amount $R - \sqrt{R^2 - E^2}$ to ensure the target facet remains at the focal point of Lens 2.

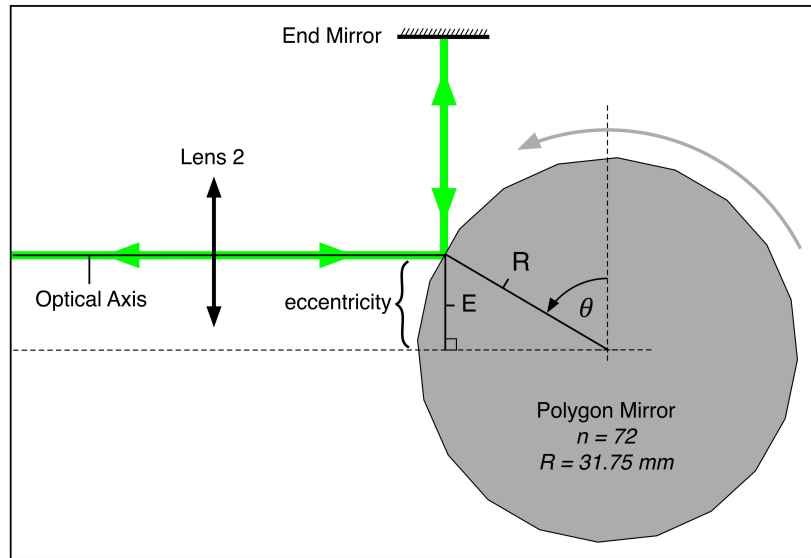


Figure 5. Eccentricity E has been introduced to improve the instantaneous linewidth. The beams now retro-reflect off an end mirror before travelling back through the filter. The visible facet width consequently decreases with increasing eccentricity until $E = R$ whereby the visible facet width reduces to zero.

For the beam travelling along the telescope axis (of central wavelength λ_c), the visible width of the facet l_v is given by $a \sin \theta$, where θ is the rotational angle of the polygon and is related to the eccentricity by $\theta = \cos^{-1} \left(\frac{E}{R} \right)$, therefore the expression for l_v is

$$l_v = 2R \sin \left(\frac{\pi}{n} \right) \sin \left(\cos^{-1} \left(\frac{E}{R} \right) \right) \quad (5)$$

3. RESULTS

With a fixed radius, a higher number of facets will result in smaller facet widths, accommodating smaller beam widths only. With these considerations in mind we can begin to investigate how the accepted beam width changes depending on the properties of the PM. For a given PM, the apothem R is a constant, while different incident beam widths can be calculated and plotted for different numbers n of facets. The eccentricity E (normalized to the polygon apothem R) provides the parameter for the family of curves in Figure 6.

These graphs provide an immediate visualisation of the extent to which the visible facet width can be made larger when reducing the number of facets, which has a greater impact for smaller values of n . The widest visible facet width occurs at $\theta = 90^\circ$ when the PM is positioned exactly on-axis and reduces to zero when the eccentricity, $E = R = 31.75$ mm, as expected. What is less intuitive however is the minute changes in the visible facet width for a higher number of facets. The eccentricity should be made as low as possible to reduce the ratio of E/R as much as possible if the widest visible facet is to be achieved.

The converging angle ψ of an on-axis polygon is equal to the acceptance angle φ of the polygon (Fig. 2) but it is double the acceptance angle when the PM is placed off-axis ($E > 0$). This is due to the existence of an incidence angle and reflectance angle instead of just reflecting at normal incidence only. The whole spectrum must be distributed over twice the acceptance angle or less to be successfully and completely tuned from λ_{max} to λ_{min} . Any light propagating outside of the converging angle will not strike the facets at the correct angle to reflect at normal incidence off the end mirror and therefore will not be recaptured.

The off-axis positioning of the PM in our setup, resulting in a doubled converging angle, means that the marginal rays can converge onto the polygon from Lens 2 over a maximum angular displacement of $\psi = 4\pi/n$ or 10° , allowing the beams at λ_{min} and λ_{max} to have a maximum of 5° incidence angle either side of the optical axis (Fig. 7). The visible facet width is reduced for the marginal beam travelling below the optical axis, in comparison to the beam travelling above, and we know that the widest beam width occurs for the shortest wavelength. Therefore, Equation 4 must be modified to accommodate the shortest wavelength incident on the facet due to the maximum converging angle.

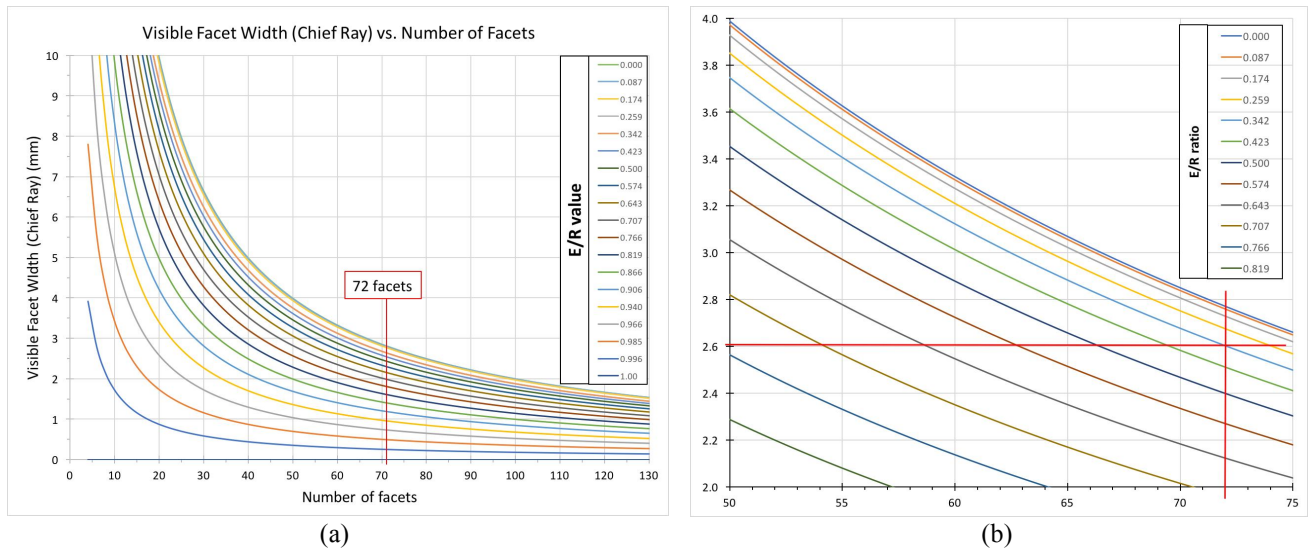


Figure 6. (a) The visible facet widths for the wavelength propagating along the telescope optical axis as a function of the number of facets, ranging from 4 to 130. Each parametric curve corresponds to a different ratio of E/R where zero indicates that the polygon is positioned exactly on-axis and 1 indicates that the facet is perpendicular to the incident beam, reflecting zero light. A higher facet count yields the smallest change in visible facet width over the range of eccentricities. Our PM has been indicated by a vertical line at 72 facets. (b) An enlargement of the region situated around our PM with the vertical and horizontal lines crossing at the location of our setup's current arrangement.

The angle β_{min} is the 5° angle between the optical axis and the marginal beam for λ_{min} . This angle should be subtracted from the polygon rotation angle θ . Another aspect that must be taken into consideration is the fact that the facet angle changes as the polygon sweeps through the spectrum. A single sweep occurs over $5^\circ \left(\frac{2\pi}{n}\right)$, moving $2.5^\circ \left(\frac{\pi}{n}\right)$ either side of the central wavelength from λ_{max} to λ_{min} . When the PM is tuning the shortest wavelength λ_{min} , the facet is rotated 2.5° towards the incident beam, meaning that this angle should be added back onto the rotation angle to find the correct visible facet width.

$$l_v = a \sin \left(\theta - \beta_{min} + \frac{\pi}{n} \right) = 2R \sin \left(\frac{\pi}{n} \right) \sin \left(\cos^{-1} \left(\frac{E}{R} \right) - \frac{\pi}{n} \right). \quad (6)$$

Equation 6 represents the maximum beam width that can be accommodated on the facet, which in the case of the “below axis” configuration occurs at the short wavelength end of the spectrum.

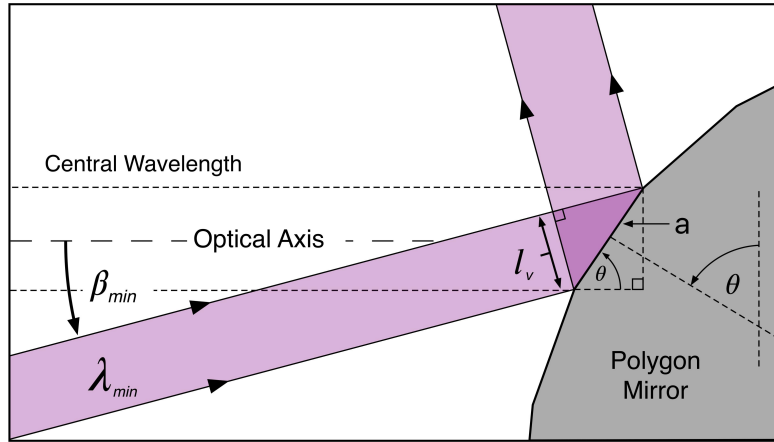


Figure 7. The marginal beam for λ_{min} falls incident onto the facet of width a at an angle $\beta_{min} = 2\pi/n$ from the optical axis, which reduces the visible facet width l_v . This must be subtracted from the PM rotation angle θ but the PM must also rotate counter clockwise by π/n to tune the wavelength λ_{min} , which means that equation 4 must also include the addition of π/n to the PM rotation angle θ to obtain the correct visible facet width.

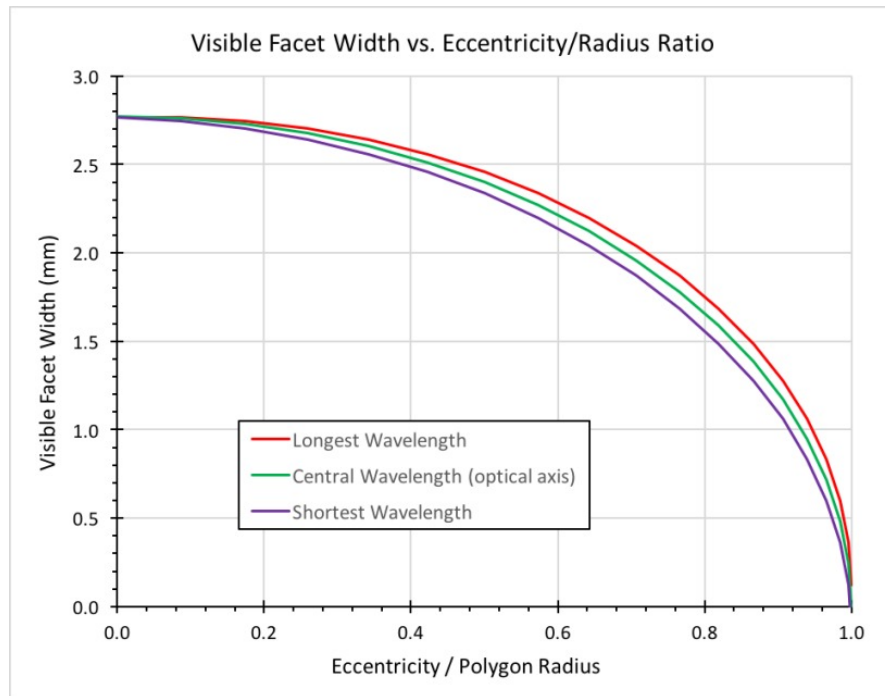


Figure 8. Visible facet width as a function of the ratio E/R as seen by the longest wavelength λ_{max} (top), the central wavelength λ_c (middle) and the shortest wavelength λ_{min} (bottom). The difference in visible facet width, between λ_{max} and λ_{min} , gradually increases as E/R ranges from zero to 1. Minimum PM eccentricity is required to ensure that minimal changes in visible facet width occur for all wavelengths.

The parametric graph in Figure 8 highlights the reduction in visible facet width with increasing eccentricity (as a fraction of PM apothem). The three curves correspond to the longest wavelength λ_{max} (top), the central wavelength λ_c (middle) and the shortest wavelength λ_{min} (bottom). These wavelength values are dictated by the need to accommodate the spectrum, which is itself governed by the acceptance angle of the polygon, rather than being the bandwidth limits of the light source.

4. CONCLUSIONS

Reducing the eccentricity from the current value of nearly 0.33 to 0 results in only a very small improvement in the visible facet width ($\sim 100\ \mu\text{m}$) and there is a much higher impact when the number of facets is reduced while keeping the radius of the polygon fixed. The visible facet width can be increased by about 23% by employing a PM with 25% fewer facets. However, the shape of such a PM would depart from a circle more markedly with fewer facets, which would be detrimental to the operation at higher speeds. It is conceivable that the reduction in speed would therefore be more than 25%. Additionally, the way in which each facet pivots around the centre of the PM results in more pronounced duty cycle limitations that need to be examined separately¹⁰.

In Figure 7 we determined how wide the beam can be in order to avoid vignetting at the facet, which for the “below axis” setup presented in our paper will occur for the shorter wavelengths. The λ_{min} beam cannot be wider than the limit given in Equation 6, which dictates the choice of telescope lens combination.

With the PM positioned below axis, the shortest wavelength, with the widest beam width, falls onto a narrower visible facet width than the longest wavelength. The visible facet width decreases with increasing eccentricity and falls more rapidly for the shortest wavelength. The extent to which both marginal wavelengths fit onto the PM facet diverges for increasing eccentricity, which has the effect of skewing the recaptured spectrum towards the longer wavelengths. Placing the PM in the “above-axis” position is more suited to capturing the wider beam at short wavelengths, thereby reversing this skew, but in doing so the direction of sweep is reversed. This is desirable for the added reason that short to long wavelength sweep direction is favoured in swept lasers^{11, 12}.

ACKNOWLEDGMENTS

Mike Everson would like to thank the Engineering and Physical Sciences Research Council (EPSRC) for funding the project. George Dobre and Virgil-Florin Duma acknowledge the support of the Romanian National Authority for Scientific Research, CNDI–UEFISCDI project PN-III-P2-2.1-PED-2016-1937 (<http://3om-group-optomechatronics.ro/>).

REFERENCES

- [1] Choma, M., Sarunic, M., Yang, C., and Izatt J., “Sensitivity advantage of swept source and Fourier domain optical coherence tomography,” *Opt. Express* 11, 2183–2189 (2003).
- [2] Duma, V.-F. and Podoleanu, A. Gh., “Polygon mirror scanners in biomedical imaging: a review,” *Proc. SPIE* 8621, 8621V (2013).
- [3] Wieser, W., Klein, T., Draxinger, W., and Huber, R., “Fully automated 1.5 MHz FDML laser with 100 mW output power at 1310 nm,” *European Conference on Biomedical Optics* (p. 954116). Optical Society of America (2015).
- [4] Oh, W. Y., Vakoc, B. J., Shishkov, M., Tearney, G. J., and Bouma, B. E., “> 400 kHz repetition rate wavelength-swept laser and application to high-speed optical frequency domain imaging,” *Opt. Letters* 35(17), pp.2919-2921 (2010).
- [5] Mao, Y., Chang, S., Murdock, E., and Flueraru, C., “Simultaneous dual-wavelength-band common-path swept-source optical coherence tomography with single polygon mirror scanner,” *Opt. Letters* 36(11), 1990-1992 (2011).
- [6] Everson, M., Duma, V.-F., and Dobre, G., “Geometric & radiometric vignetting associated with a 72-facet, off-axis, polygon mirror for swept source optical coherence tomography (SS-OCT),” *AIP Conference Proceedings* 1796, 040004 (2017).
- [7] Everson, M., Duma, V.-F., Dobre, G., “Optical power transmission in a polygon mirror-based swept source optical coherence tomography system,” *Proc. SPIE* 10335, 1033520 (2017).
- [8] Mao, Y., Flueraru, C., Sherif, S., and Chang, S., “High performance wavelength-swept laser with mode-locking technique for optical coherence tomography,” *Opt. Communications* 282(1), 88-92. (2009).
- [9] Oh, W. Y., Yun, S. H., Tearney, G. J., and Bouma, B. E., “115 kHz tuning repetition rate ultrahigh-speed wavelength-swept semiconductor laser,” *Opt. Letters* 30(23), 3159-3161 (2005).

- [10] Duma V.-F., "Polygonal mirror laser scanning heads: Characteristic functions," Proceedings of the Romanian Academy Series A 18(1), 25-33 (2017).
- [11] Johnson, B., Atia, W., Kuznetsov, M., Goldberg, B. D., Whitney, P., and Flanders, D. C., "Analysis of a spinning polygon wavelength swept laser," *arXiv preprint arXiv:1501.07003* (2015).
- [12] Chong, C., Suzuki, T., Morosawa, A., and Sakai, T., "Spectral narrowing effect by quasi-phase continuous tuning in high-speed wavelength-swept light source," Opt. Express 16(25), 21105-21118 (2008).